8-2021

Covalent Immobilization of Molecular Complexes on Metal-Organic Frameworks Towards Robust and Highly Efficient Heterogeneous Water Oxidation Catalysts

Xiangming Liang
Lanzhou University

Sizhou Yang
Marquette University

Junyi Yang
Lanzhou University

Wanjun Sun
Lanzhou University

Xiangyang Li
Lanzhou University

See next page for additional authors

Applied Catalysis B: Environmental, Vol. 291 (2021, August): 120070. DOI.

Covalent Immobilization of Molecular Complexes on Metal-Organic Frameworks Towards Robust and Highly Efficient Heterogeneous Water Oxidation Catalysts

Xiangming Liang
State Key Laboratory of Applied Organic Chemistry, Key Laboratory of Nonferrous Metals Chemistry and Resources Utilization of Gansu Province, and College of Chemistry and Chemical Engineering, Lanzhou University, China
Sizhou Yang
Department of Chemistry, Marquette University, Milwaukee, WI, 53201, United States
Junyi Yang
State Key Laboratory of Applied Organic Chemistry, Key Laboratory of Nonferrous Metals Chemistry and Resources Utilization of Gansu Province, and College of Chemistry and Chemical Engineering, Lanzhou University, China
Wanjun Sun

State Key Laboratory of Applied Organic Chemistry, Key Laboratory of Nonferrous Metals Chemistry and Resources Utilization of Gansu Province, and College of Chemistry and Chemical Engineering, Lanzhou University, China

Xiangyang Li
State Key Laboratory of Applied Organic Chemistry, Key Laboratory of Nonferrous Metals Chemistry and Resources Utilization of Gansu Province, and College of Chemistry and Chemical Engineering, Lanzhou University, China

Baochun Ma
State Key Laboratory of Applied Organic Chemistry, Key Laboratory of Nonferrous Metals Chemistry and Resources Utilization of Gansu Province, and College of Chemistry and Chemical Engineering, Lanzhou University, China

Jier Huang
Department of Chemistry, Marquette University, Milwaukee, WI, 53201, United States

Jiangwei Zhang
Dalian National Laboratory for Clean Energy & State Key Laboratory of Catalysis, Dalian Institute of Chemical Physics, Chinese Academy of Sciences (CAS), Dalian, China

Lele Duan
Department of Chemistry, Shenzhen Grubbs Institute and Guangdong Provincial Key Laboratory of Energy Materials for Electric Power, Southern University of Science and Technology, Shenzhen, Guangdong, China

Yong Ding
State Key Laboratory of Applied Organic Chemistry, Key Laboratory of Nonferrous Metals Chemistry and Resources Utilization of Gansu Province, and College of Chemistry and Chemical Engineering, Lanzhou University, China

Abstract

The major challenges to practical implementation of efficient noble metal based molecular water oxidation catalysts are their stability and recycle ability. Herein, noble metal Ru based molecular water oxidation catalysts were covalently anchored in MOFs through “amide bond” as bridges, which leads to the formation of high-efficiency and robust heterogeneous catalysts for water oxidation reaction. We show that the efficiency for Ce^{IV}-driven water oxidation was significantly enhanced by 120 times when the Ru molecules were immobilized on the frameworks of MIL-101(Cr). The relationship between recycle stability and the structure of the Ru complexes covalently anchored in MOFs was carefully studied by recycle tests and various characterization methods. $[Ru(terpy)(pic)_2(H_2O)]^{2+}$ was directly certified as real catalytic species instead of the original complex $[Ru(terpy)(pic)_2Cl]^{+}$ by the X-ray absorption spectroscopy and control experiments. The synthetic method of hybrid catalysts offers a good strategy for enhancing water oxidation activity and stability of molecular catalysts.

Graphical abstract

The noble metal Ru based molecular water oxidation catalysts were covalently anchored in MOFs through “amide bond” as bridges, which leads to the formation of high-efficiency and robust heterogeneous catalysts for water oxidation reaction.

Building a Ship (Ru complexes) in a Bottle (MOFs)

Keywords

Covalent immobilization, Water oxidation, Metal-organic framework, Molecular complex

1. Introduction

The current energy and environment crisis have stimulated the development of clean and renewable energy [[1], [2], [3]]. Hydrogen evolution from water splitting is a promising method to address the energy and environmental problems [4] because hydrogen possesses high heat value and combusts to water as the only product [[5], [6], [7]]. Water splitting consists of two half reactions, water oxidation and water reduction, where the former is believed to be the bottleneck due to the required transfer process of multiple protons and electrons [[8], [9], [10], [11]]. As a result, considerable efforts have been made on developing water oxidation catalysts (WOCs) over the past few decades [[12], [13], [14], [15], [16]]. The WOCs can be either heterogeneous catalysts, such as metal oxides [[17], [18], [19], [20]] and metal sulfides [[21], [22], [23], [24]], or homogeneous catalysts, such as metal complexes [[25], [26], [27], [28], [29], [30]] and polyoxometalates (POMs) [[31], [32], [33], [34], [35]]. Numerous heterogeneous catalysts have been studied in detail, and a great many of rewarding achievements have been achieved [[36], [37], [38], [39]]. Although heterogeneous catalysts are stable and convenient for recycling, it is challenging to enhance the catalytic ability of oxygen evolution for them by systematically chemical modification, and the catalytic mechanisms of heterogeneous catalysts are difficult to verify. Therefore, it is necessary to develop homogeneous catalysts which have shown considerable advantages in terms of catalytic activity regulation through great superiority in studying the reaction mechanism and improving the catalytic activity [[40], [41], [42], [43], [44]]. However, the vital challenges of recovery and stability limited the development of homogeneous catalysts.

Since the “blue dimer” was used as homogeneous WOC in 1982, various ruthenium complexes with robust structures and high activities were developed for catalytic water oxidation [[45], [46], [47], [48], [49], [50]]. Some heterogeneous metal oxides derived from the decomposition of molecular catalysts were found to be the true catalytic species for water oxidation [51]. Unprotected molecular catalysts are easily decomposed under harsh water oxidation conditions. The photosystem II of the nature elegantly solved the robustness challenge of oxygen-evolving complex by embedding the [Mn_4CaO_5] cluster into protein environments [52]. This protein-encapsulated [Mn_4CaO_5] cluster effectively protects oxygen-evolving complex from aggregation and degradation and provides favorable electronic environments for multiple redox steps of water oxidation. The combination of molecular cluster and the stabilizing support is essential for natural system and offers a promising method to realize the recovery and enhancement of stability for homogeneous catalysts. At present, it is a challenge to covalently anchor homogeneous WOCs on support to form effective heterogeneous catalyst. POMs as homogeneous catalysts are difficult to achieve the heterogenization due to the lack of modifiable sites. Metal complexes, another important type of homogeneous catalysts, can be chemically modified to anchor to the heterogeneous materials with covalent bond, so as to realize the heterogenization of homogeneous catalysts.

Compared with other heterogeneous materials, metal-organic frameworks (MOFs) show advantages in the pore volume, specific surface area and tunable chemical environments in cavities of MOFs, which can be modified by post-synthetic treatment [[53], [54], [55]]. These features make MOFs suitable to provide appropriate chemical environments and abundant anchoring sites for homogeneous catalysts. Herein, inspired by the natural strategy, we used MOFs as the support of homogeneous catalysts and developed a new covalently anchoring strategy by introducing easily synthetic amide bond as a bridge connecting metal complexes and MOFs. MIL-101(Cr) has great advantages in appropriate sizes of pore volume and excellent chemical stability [56] so that it was chosen as the support of homogeneous catalysts. Two homogeneous catalysts $[Ru(terpy)(pic)_3](PF_6)_2$ (terpy = 2,2';6',2"-terpyridine, pic = 4-picoline) (**1**) and $[Ru(terpy\text{-}Ac)(pic)_3](PF_6)_2$ (terpy-Ac = [2,2':6',2"-terpyridine]-4'-carboxylic acid) (**2**) were synthesized as a control group, and three covalently anchored, proof-of-concept heterogeneous catalysts MIL-101(Cr)-$[Ru(terpy\text{-}Ac)(pic)_2Cl](PF_6)$ (**3**), MIL-101(Cr)-$[Ru(terpy)(isc)Cl_2]$ (isc = isonicotinic acid) (**4**), MIL-101(Cr)-$[Ru(terpy)(isc)(pic)_2](PF_6)_2$ (**5**) were successfully prepared to prove the above mentioned state-of-the-art strategy (Fig. 1). The kinetics of Ce^{IV}-driven ($Ce^{IV} = Ce(NH_4)_2(NO_3)_6$) water oxidation catalyzed by these catalysts were investigated in detail. Water oxidation efficiency was significantly enhanced by 120 times when the Ru molecules were immobilized on the frameworks of MIL-101(Cr). The catalysts **3** and **4** were certified as the robust water oxidation catalysts while catalyst **5** exhibited poor stability in recycle tests. Mechanistic studies revealed that the water oxidation activity and stability of these catalysts were closely related to the coordination structure of molecular species anchored in MIL-101(Cr) and the real catalytic species was directly certified as Ru aqua species, $[Ru{-}OH_2]$, as evidenced by X-ray absorption spectroscopy (XAS).

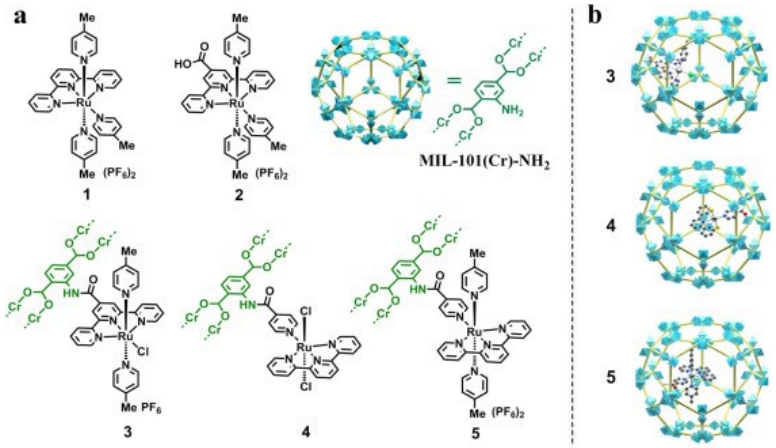

Fig. 1. (a) The structures of catalysts studied in this paper. (b) Schematic representations of catalysts **3**, **4** and **5**.

2. Experiment section

2.1. Materials

All salts and other chemicals were of the highest purity available from commercial sources without further purification. Purified water (18.25 MΩ cm applied in all the experiments was attained from a Molecular Lab Water Purifier.

2.2. Synthesis of heterogeneous catalysts

As shown in Scheme 1, 0.6 g (2.2 mmol) 2,2':6',2"-terpyridine-4'-carboxylic acid (terpy-Ac) in 10 mL thionyl chloride ($SOCl_2$) was heated under reflux for 4 h. After that, evaporation of $SOCl_2$ resulted in white precipitate (**7**). Then, 20 mL dichloromethane (CH_2Cl_2) suspension of 0.4 g the obtained white precipitate, 0.4 g MIL-101(Cr)-NH_2 and 0.8 mL triethylamine was degassed with argon and refluxed for 24 h. The solid was centrifuged and washed with EtOH and CH_2Cl_2 for three times. The collected solid was dried at room temperature to give MIL-

101(Cr)-terpy-Ac (**8**). A mixture of 0.2 g **8** and 0.12 g (0.6 mmol) $RuCl_3 \cdot xH_2O$ in 30 mL EtOH was heated under reflux for 20 h. Then the solid was centrifuged and washed with water and ethanol, respectively. The collected solid was dried in vacuum to give MIL-101(Cr)-Ru(terpy-Ac)Cl_3 (**9**). A suspension of 0.2 g **9**, 1.5 mL (15 mmol) 4-picoline, 0.3 mL triethylamine and 0.02 g (0.47 mmol) LiCl in EtOH/H_2O (v:v = 1:1) was degassed and heated to reflux for 24 h. The solid was centrifuged and added into 6 mL H_2O. Then, excess NH_4PF_6 was added into the suspension solution. The black solid was collected and washed five times with water, ethanol and CH_2Cl_2 to yield MIL-101(Cr)-[Ru(terpy-Ac)$(pic)_2$Cl](PF_6) (**3**). Terpy-Ac (**6**) was substituted by isonicotinic acid (**10**) to connect MIL-101(Cr)-NH_2 with molecular Ru catalysts, and similar synthetic routes were used to prepare **4** and **5** (Scheme 1b).

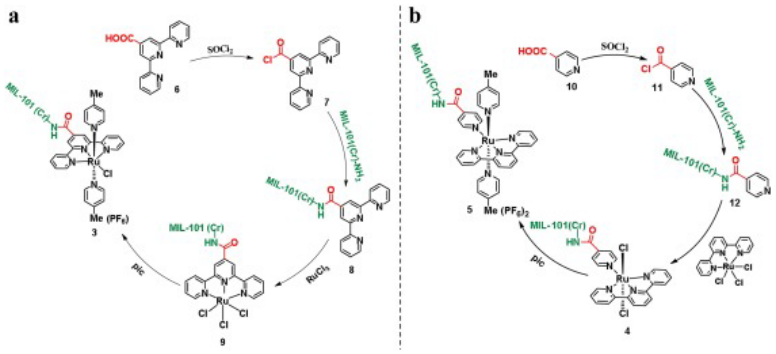

Scheme 1. The synthesis routes of catalyst **3** (a), catalysts **4** and **5** (b).

3. Results and discussion

3.1. Synthesis and Characterization

Complex **1** was synthesized according to the method of previous literature (Figs. S1-S2) [57]. The new complex **2** was characterized by ^{1}H NMR (Fig. S5), ^{13}C NMR (Fig. S6), UV–vis spectroscopy (Fig. S7) and FT-IR spectrum (Fig. S8). In order to obtain the designed catalysts, a simple condensation reaction between the carboxyl group on terpy-Ac (**6**) and the amino group on MIL-101(Cr)-NH_2 was incipiently used to connect terpy-Ac with the MIL-101(Cr)-NH_2 in the presence of N,N'-diisopropylcarbodiimide as catalyst. However, this method failed due to the low reactivity between the carboxyl and amino groups. Then, a new strategy was developed. As shown in Scheme 1a, the amide bond could be easily achieved by the reaction of acid chloride and amino group. Thereby, [2,2':6',2"-terpyridine]-4'-carbonyl chloride (**7**) was synthesized and used to react with MIL-101(Cr)-NH_2. As expected, **7** and MIL-101(Cr)-NH_2 successfully reacted and afforded **8**. Next, **9** was obtained by the simple reflux treatment of **8** and $RuCl_3$. Catalyst **3** was eventually synthesized after the replacement of two axial chlorides in **9**. Catalysts **4** and **5** were designed to provide more direct evidence for illustrating the structure-activity relationship in water oxidation. The as-obtained hybrid products **3**, **4** and **5** were characterized by powder X-ray diffraction (XRD) (Fig. S9), transmission electron microscopy (TEM) and scanning electron microscopy (SEM). As shown in Fig. 2, all samples retain the octahedral morphology after incorporation. After comparing the XRD patterns with previously reported MIL-101(Cr), it seems that the crystallinity of hybrid MOFs decreased, which is likely due to the loading of Ru guests that introduces the disorder of the framework and weakens the diffraction. The successful incorporation Ru catalysts was confirmed by monitoring ^{1}H NMR of digest hybrid MOF, MIL-101(Cr) and MIL-101(Cr)-NH_2, where we observed the formation of amide N─H at 12.5 ppm and the presence of aromatic peaks appeared at 7.77, 7.75, 7.38, 7.02, 7.00 ppm from the 2-aminoterephthalic acid (H_2BDC-NH_2) compared to MIL-101(Cr) (Fig. S10). Moreover, the mass spectrometry of digested **8** shows evident ion peaks at *m/z* 441.1241 and 463.1062, which are assigned to [H_2BDC-NHCO-terpy + H]$^+$ (calculated *m/z*, 441.12) and [H_2BDC-NHCO-terpy + Na]$^+$ (calculated *m/z*, 463.10), respectively (Fig. S11). The presence of Ru complex was further supported by diffuse reflectance UV–vis spectroscopy. As shown in Fig. S12, the additional absorption in the range 436−595 nm in samples **3**, **4** and **5** compared to MIL-101(Cr) is consistent

with the absorption feature of Ru complexes **1** and **2** and thus can be attributed to the presence of Ru complexes from incorporation. Besides, the molecular Ru complexes are distributed uniformly in cavities of MIL-101(Cr) according to the elemental mapping images and the high-angle annular dark-field scanning transmission electron microscopy (HAADF-STEM) (Fig. 2). FT-IR spectra of **3**, **4** and **5** exhibit high similarity to that of MIL-101(Cr)-NH_2 (Fig. S8). Distinct vibration peaks found at 1395 cm^{-1} and 1621 cm^{-1} are due to the asymmetric vibration of carboxylate present in the frameworks of MIL-101(Cr) [58]. The apparent characteristic peaks of molecular catalysts are not observed in the FT-IR spectra, due to the relatively low loading of Ru complexes in MIL-101(Cr)-NH_2.

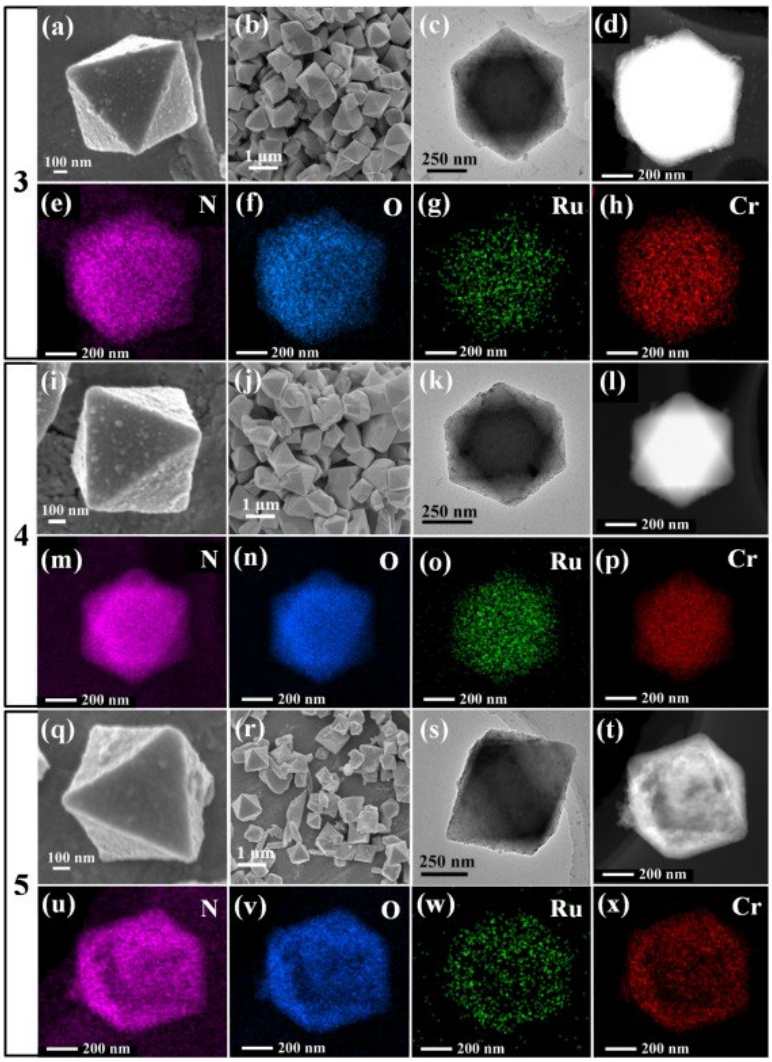

Fig. 2. SEM of fresh **3** (a, b), fresh **4** (i, j) and **5** (q, r), TEM of fresh **3** (c), fresh **4** (k) and fresh **5** (s), HAADF-STEM of fresh **3** (d), fresh **4** (l) and **5** (t), corresponding elemental mapping images of fresh **3** (e-h), fresh **4** (m-p) and **5** (u-x).

In addition to the bulk structure, the local coordination environments of the Ru center were confirmed by XAS. The X-ray absorption near edge structure (XANES) spectra of catalysts **3**, **4**, **5** and four reference samples, i.e. Ru foil, $[Ru(bpy)_3]Cl_2$ (bpy = 2,2'-bipyridine), $RuCl_3$ and dichloro(p-cymene)ruthenium(II) dimer (D-Ru), are shown in Fig. 3a. The main feature at ~22.123 keV in the spectrum of $[Ru(bpy)_3]Cl_2$ is the absorption white line corresponding to the dipole allowed 1s-5p transition. The lack of pre-edge feature implies the centrosymmetric geometry of $[Ru(bpy)_3]Cl_2$, which is consistent with literature reports [59,60]. Similar spectral features were observed for catalysts **3**, **4** and **5**, suggesting that the Ru center likely processes octahedral geometry after

incorporation. Moreover, the edge energy of XANES spectra of catalysts **3**, **4** and **5** as shown in the first derivative XANES spectra exhibit excellent agreement with $[Ru(bpy)_3]Cl_2$ reference, implying that the Ru center in MIL-101(Cr) retains +2 oxidation state. In order to confirm that catalysts **3**, **4** and **5** have good dispersion in the frameworks of MOFs, the Fourier transform (FT) of k^2-weighted χ(k) space spectra into radial distance χ(R) space spectra is conducted as an intuitive method. From the χ(R) spectra of **3**, **4**, **5** and the references, the peak located at 1.85 Å is the scattering path of characteristic Ru—N bonding in $[Ru(bpy)_3]Cl_2$. The scattering path of Ru—Cl bonding in $RuCl_3$ and D-Ru is located at 2.21 Å. As shown in Fig. 3b and Fig. S16, the peaks of Ru—N bonding appear in catalysts **3**, **4** and **5** while the peaks of Ru—Cl bonding only appear in **3** and **4**. The most prominent peak located at 2.64 Å is the scattering path of Ru—Ru bonding in Ru foil. It should be pointed out that the weak peak located at 2.68 Å is the scattering path of Ru—N—C bonding in the second coordination shell of Ru complex segment in catalyst **5**. The characteristic peak of Ru—Ru metal bonding is not obvious in catalysts **3**, **4** and **5**, which supports the good dispersion of Ru atoms in MOFs.

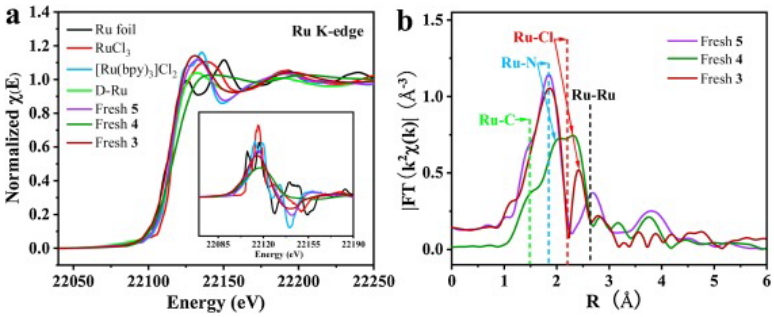

Fig. 3. (a) Normalized K edge X-ray absorption near edge structure (XANES) χ(E) spectra. The inset is the first derivative XANES spectra. (b) Radial distance χ(R) space spectra of fresh catalysts, the dotted lines represent the radial distance of the Ru—C bond in D-Ru (green), Ru—N bond in $[Ru(bpy)_3]Cl_2$ (light blue), Ru—Cl bond in $RuCl_3$ (red) and Ru—Ru bond in Ru foil (black) (For interpretation of the references to colour in this figure legend, the reader is referred to the web version of this article.).

The wavelet transform of χ(k) is an effective approach to investigate the coordination environment of Ru atoms in MOFs especially for the situation that the local structure of metal atoms with "hybrid atoms" coordination environment in the first coordination shell [61]. From the wavelet transform of χ(k) spectra of catalysts **3**, **4** and **5**, the scattering path signal located at [χ(k), χ(R)] of [5.60, 1.86] is assigned to Ru—N and the subtle signal located at [χ(k), χ(R)] of [7.20, 2.30] is Ru—Cl, revealing that the coordination environment of Ru atoms in **3** contains Ru—N and Ru—Cl (Fig. 4). Similarly, the distinct signal located at [χ(k), χ(R)] of [8.40, 2.20] indicates that both Ru—N and Ru—Cl are coexisted in **4** while the two closed scattering path signals merged (Fig. S17a). For catalyst **5**, the evident signal of Ru—N bonding in the first coordination shell locates at [χ(k), χ(R)] of [5.40, 1.86] while a weak signal of Ru—C in the second coordination shell locates at [χ(k), χ(R)] of [6.31, 2.63] (Fig. S17b). Moreover, the signal of Ru—Ru bonding in Ru foil located at [χ(k), χ(R)] of [9.60, 2.64] is not observed in catalysts **3**, **4** and **5**, which further testifies the good dispersion of Ru molecules in MOFs.

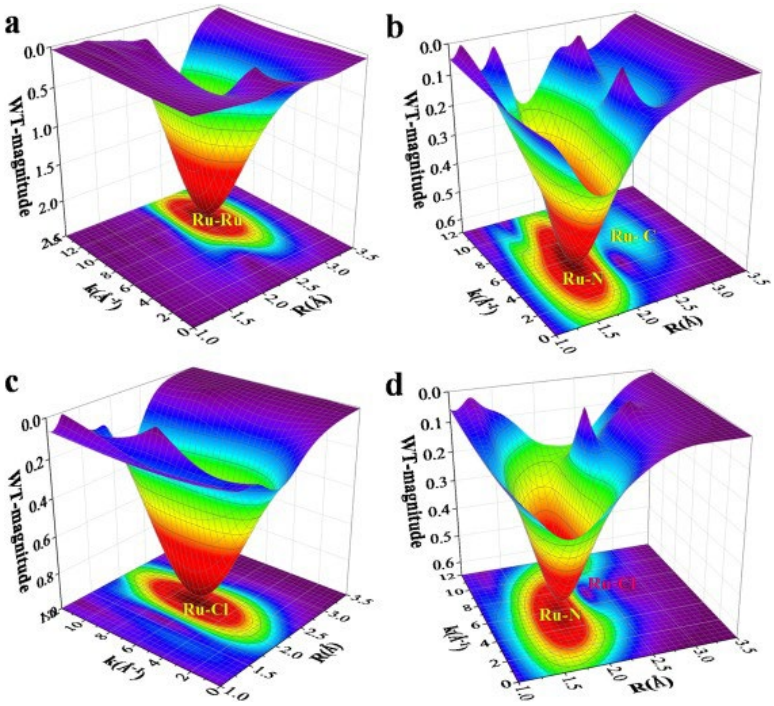

Fig. 4. Wavelet transform extended X-ray absorption fine structure (WTEXAFS) of Ru foil (a), $[Ru(bpy)_3]Cl_2$ (b), $RuCl_3$ (c) and Catalyst **3** (d).

To gain a better understanding of the local coordination environment, we quantitatively fitted the extended X-ray absorption fine structure (EXAFS) spectra of catalysts **3**, **4** and **5**. As shown in Fig. 5, fitting models based on synthetic scheme and wavelet transform results were used to fit the data. The fitting parameters were summarized in Table S1-S3. The first coordination shell of Ru in catalyst **3** exhibits Ru—N and Ru—Cl bonding with coordination number approaching 5.0 and 1.0 (Table S1). The quantitative χ(R) space spectrum of fresh **3** fits well to the DFT-optimized structure model of $[Ru(terpy\text{-}Ac\text{-}NH_2)(pic)_2Cl]^+$. In the same way, the first coordination shell of Ru in catalyst **4** displays Ru—N and Ru—Cl bonding with coordination number approaching 4.0 and 2.0 (Table S2). The quantitative χ(R) space spectrum of fresh **4** fits well to the DFT-optimized structural model of $[Ru(terpy)(isc\text{-}NH_2)Cl_2]$. Catalyst **5** only exhibits Ru—N bonding with coordination number approaching 6.0 in the first coordination shell of Ru (Table S3). The quantitative χ(R) space spectrum of fresh **5** fits well to the DFT-optimized structural model of $[Ru(terpy)(isc\text{-}NH_2)(pic)_2]^{2+}$. Thus, the core structures of the Ru units in catalysts **3**, **4** and **5** are $[Ru(terpy\text{-}Ac)(pic)_2Cl]^+$, $[Ru(terpy)(isc)Cl_2]$ and $[Ru(terpy)(isc)(pic)_2]^{2+}$, respectively. The average Ru contents in catalysts **3**, **4** and **5** were ca. 3.86 wt%, 2.83 wt% and 2.32 wt% detected by inductively coupled plasma-optical emission spectroscopy (ICP-OES) (Table S5). The pore windows of MIL-101(Cr) are important to provide passages of ligand terpy or pic into MOFs, and therefore critical for in-situ synthesis of catalysts. 12 Å pentagonal windows and 16 Å hexagonal windows of MIL-101(Cr) are large enough to allow the free pass for terpy-Ac and pic (Figs. S18-S19). The longest sizes of molecular models optimized by DFT in catalysts **3**, **4** and **5** are 14.29 Å, 14.08 Å and 13.75 Å (Figs. S20-S22), respectively. Molecular catalysts are easily formed in situ in MOFs due to the large size of MOF cages [62]. In addition, the similar sizes between molecular catalysts and the windows of MOFs are helpful to maintain the molecular catalysts in the cages of MOFs.

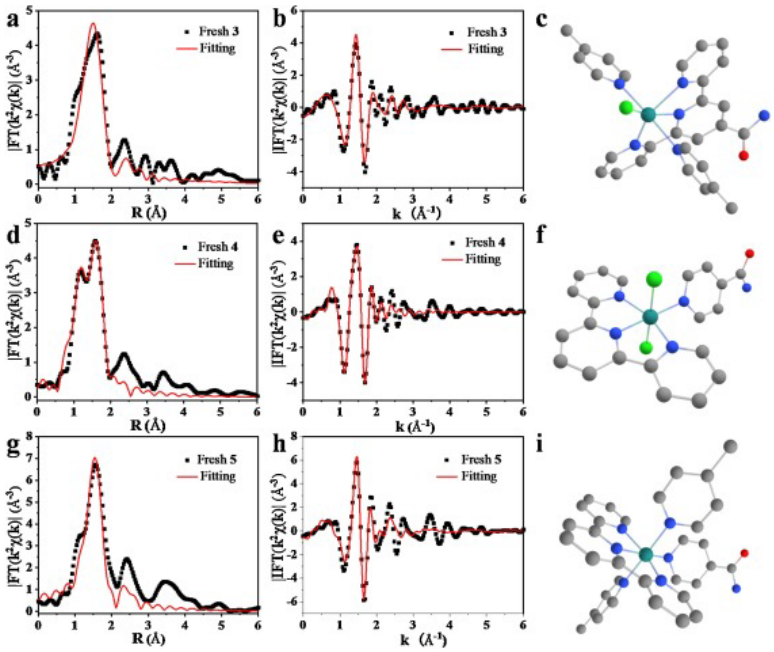

Fig. 5. χ(R) space spectra fitting curves of **3** (a), **4** (d) and **5** (g), inverse FT χ(R) space spectra into χ(q) space spectra (χ(k) space) fitting curves of **3** (b), **4** (e) and **5** (h) at Ru K-edge, the red lines are the fit to the DFT-optimized molecular model $[Ru(terpy\text{-}Ac\text{-}NH_2)(pic)_2Cl]^+$ (c), $[Ru(terpy)(isc\text{-}NH_2)Cl_2]$ (f) and $[Ru(terpy)(isc\text{-}NH_2)(pic)_2]^{2+}$ (i). C (gray), H (light gray), O (red), N (blue), Ru (dark cyan), Cl (green) (For interpretation of the references to colour in this figure legend, the reader is referred to the web version of this article.).

3.2. Water oxidation reaction

The catalytic activities for all catalysts were examined under excess Ce^{IV}-driven water oxidation under acidic conditions. Oxygen evolution was observed as excess Ce^{IV} was added into the deaerated aqueous solutions of catalysts (pH 1.0). The oxygen evolution kinetics of different catalysts was investigated (Fig. 6).

Catalyst **3** showed the highest catalytic activity, and the activities follow the order **3** > **5** > **4** (Fig. 6a). Compared with fresh catalyst **3**, a simple ruthenium trichloride salt and a pristine MIL-101(Cr) show almost no oxygen evolution (Fig. 6b). For complex **1**, the TON of 3 is lower than previously reported number because of the short reaction time [57]. The catalytic activity of **1** is better than that of **2**, indicating that the electron-donating ability of ligand can improve the catalytic activity of the Ru complexes. Even though, catalyst **3** (TOF is 96 h^{-1}) containing electron-withdrawing group of amide bond (N─C=O) surprisingly displayed an extremely high enhancement of the TOF which is 120 times higher than that of molecular **2** (TOF is 0.8 h^{-1}) in initial 10 min. However, the physical mixing between MOFs and complex **2** cannot visibly improve the initial TOF for homogeneous complex **2**. These controlled experiments clearly demonstrate the unique advantage of covalent anchoring strategy in enhancing oxygen evolution efficiency.

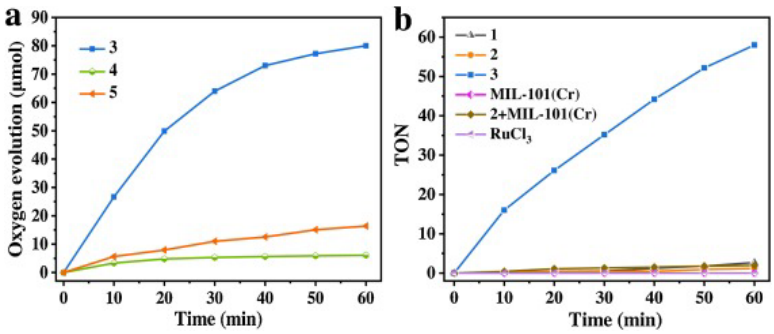

Fig. 6. (a) Kinetics of oxygen evolution in the Ce^{IV}-driven system using 10 mg heterogeneous catalysts **3**, **4** and **5**. (b) The comparison of oxygen evolution using catalysts **3** (0.66 mg, 25 μM Ru) and other catalysts (25 μM Ru and/or 0.66 mg MIL-101(Cr)), conditions: CF_3SO_3H aqueous solution (initial pH 1.0, 10 mL) containing Ce^{IV} (0.1 M); vigorous agitation using a magnetic stirrer.

The water oxidation stability of catalyst **3** was evaluated by XPS (Fig. 7), SEM, TEM, HAADF-STEM and corresponding elemental mapping images (Fig. S25). The octahedral crystals of support MIL-101(Cr) are well remained after water oxidation, indicating the good stability of MIL-101(Cr) as the supporting framework. The Ru mapping images showed that Ru was distributed uniformly in cavities of MIL-101(Cr), illustrating that the Ru complexes in catalyst **3** maintain well after water oxidation. The energy dispersive X-ray spectroscopy (EDX) analyses show that the Ru elements exist in both fresh **3** and recovered **3** (Figs. S26-S27), revealing that the covalently anchoring strategy can realize the recovery of noble metal complexes.

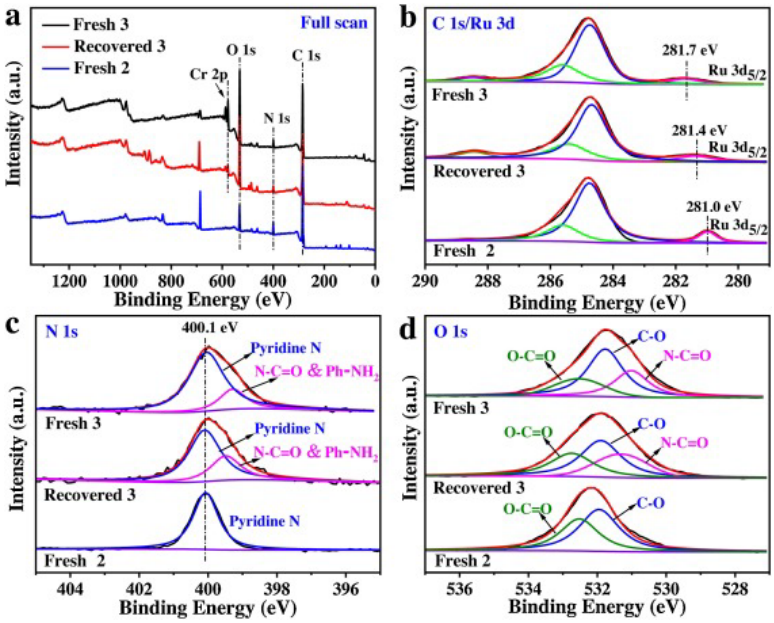

Fig. 7. XPS spectra of catalysts **2** and **3** in the energy regions of (a) full scan, (b) C 1s/Ru 3d, (c) N 1 s and (d) O 1s. The binding energy position of each sample was calibrated by the C 1s peak at 284.8 eV.

XPS spectra more informatively probe the structure and stability of the anchored Ru complex and MIL-101(Cr). For C 1s/Ru 3d spectra of catalyst **3** (Fig. 7b), two peaks located at approximately 284.8 eV and 288.4 eV are assigned to C 1s and the third one located at 281.7 eV is assigned to Ru $3d_{5/2}$. The peak of Ru $3d_{3/2}$ is positively shifted by ca. 4.2 eV vs. Ru $3d_{5/2}$ and thus overlapped with the major C 1s peak [63]. The peaks of Ru $3d_{5/2}$ for fresh **3**, recovered **3** and **2** are located at around 281.7 eV, 281.4 eV and 281.0 eV, respectively, showing that the valences of Ru in these three catalysts are +2 [[64], [65], [66]]. The Ru $3d_{5/2}$ peak of recycled **3** is negatively shifted by 0.3 eV compared with that of fresh **3**, most likely due to the change of coordination environment. The Ru $3d_{5/2}$ peak shifts to lower binding energies is generally caused by the increase in electron density of Ru [67]. The Ru $3d_{5/2}$ peak of recovered **4** is negatively shifted by 0.6 eV compared with that of fresh **4**, indicating that similar changes of coordination environment were happened in both recovered **4** and **3** (Fig. S30b). Ru $3d_{5/2}$ peak in the recovered **5** is not detected while that of fresh **5** is located at 281.5 eV, illustrating a serious leaching of Ru complex for catalyst **5** during water oxidation (Fig. S31b).

The N 1s peak of fresh molecular catalyst **2** at 400.1 eV is assigned to pyridine nitrogen (Fig. 7c). Each of N 1s bands of catalysts **3**, **4** and **5** is resolved into two peaks. The peaks of fresh **3**, **4**, **5** and recovered **3**, **4**, **5** located

at 399.9–400.2 eV are ascribed to the pyridine nitrogen (Fig. 7c, S30c, S31c). The peaks at 399.3 eV (fresh **3**) and 399.4 eV (recovered **3**) are attributed to arylamine nitrogen and amide nitrogen [68,69]. The N 1s peaks located at 399.4 eV (fresh **4**), 399.5 eV (recovered **4**), 399.3 eV (fresh **5**) and 399.1 eV (recovered **5**) are also ascribed to arylamine nitrogen and amide nitrogen. The N 1s spectra of **3**, **4** and **5** further prove that the Ru molecular catalysts are successfully immobilized in MIL-101(Cr).

The O 1s XPS spectra of **3** (before and after reaction) contain three peaks, and O 1s of catalyst **2** exhibits two peaks (Fig. 7d). The peak located at around 531.2 eV is ascribed to amide bond (N─C=O) [70], and two kinds of carboxylate groups locate at approximately 531.9 eV (C─O) and 532.6 eV (O‗C=O) [71]. The carboxylate ─groups of fresh and recovered **4** locate at around 531.8 eV (C─O) and 532.6 eV (O─C=O) (Fig. S30d). The amide bond (N─C=O) of recovered **4** is positively shifted by 0.2 eV compared with that of fresh **4**. On the contrary, the O 1s XPS spectrum of **5** after reaction is obviously changed compared with the fresh one. The O 1s spectrum of fresh **5** can be divided into three peaks at 530.8, 531.6 and 532.5 eV, corresponding to N─C=O, C─O and O─C=O (Fig. S31d). All the three peaks of O 1s are shifted to around 530.1 eV, 531.3 eV and 532.3 eV after water oxidation, suggesting the change of coordination environment of oxygen in catalyst **5**. The reason for the obvious change is very likely due to the leaching of Ru complexes and is verified in detail by the recycle test of **5**. XPS spectra further proved that although the coordination environments of Ru are altered, the Ru molecular fragments on the frame structure of MIL-101(Cr) are still retained as the form of molecules.

The stabilities of **3**, **4** and **5** were further evaluated by recycle tests (Fig. 8). Catalysts **3** and **4** maintain excellent activities as fresh catalysts after five catalytic cycles, revealing that both of them have good stability under water oxidation reaction conditions. The recycle tests of **5** exhibit a continuous decline in oxygen evolution activity, indicating a poor stability of **5**. For catalysts **3** and **4**, the supernatant solution after the first run is not active at all, however, a small quantity of oxygen is detected in supernatant of catalyst **5** after the first run, which reveals that a few Ru molecules are leached from the framework of catalyst **5** (Fig. 8d). All of the results in XPS and recycle experiments show that these catalysts have the following features: (1) **3** has the excellent oxygen evolution activity and stability comparing with other catalysts in this work. (2) For recycle tests, **4** possesses the good stability while **5** with same bridging ligand shows a sustained decrease in catalytic activity, and both of them are valuable examples for the design and synthesis of stable water oxidation catalysts in the future. (3) **5** is the worst catalyst in stability, which may be caused by the leaching of Ru complexes from the frameworks of MOFs. The comparisons among these heterogeneous catalysts certify the stability and activity of water oxidation are strongly associated with the structure of Ru complexes anchored in MOFs. It should be noted that Ce^{IV} can yield insoluble cerium oxide materials under water oxidation conditions. The resulting cerium oxide materials might gradually block the pores of MIL-101(Cr) and prevent fresh Ce^{IV} from diffusing into MOFs over time [72]. This would affect the rate of oxygen evolution and finally lead to a plateau. The adverse effects caused by cerium oxide precipitate can be eliminated in recycle tests after washing catalysts and supplying fresh Ce^{IV} solution.

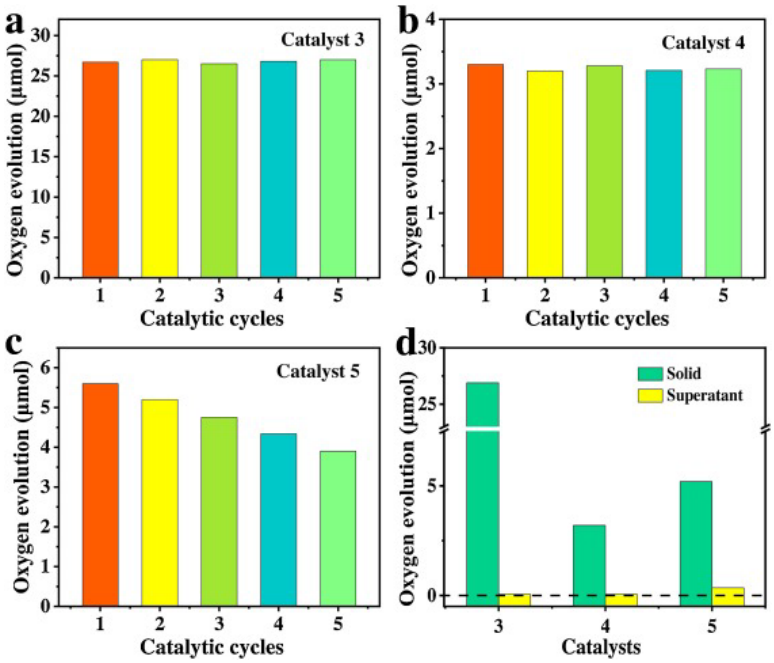

Fig. 8. Recycle tests of **3** (a), **4** (b) and **5** (c), the activities of recovered solid catalysts (10 mg) and supernatant solutions after the first run were tested by adding 0.1 M of Ce^{IV} (d), reaction time is 10 min, vigorous agitation using a magnetic stirrer.

It is impressive that a high water oxidation activity was obtained by these hybrid catalysts. The possible factors for the enhancement of catalytic activity are as follows: (1) the influence of confinement in the nanocage of MOFs; (2) the electronic effect of framework in MOFs; (3) the change of coordination environment for hybrid catalysts. The activity of the Ru complex can be greatly improved after confinement in the nanocage, while the physical mixing of complex **2** and MOFs cannot notably improve the catalytic activity of homogeneous catalysts. Local high concentration of Ru complexes can be realized due to the confinement effects in nanocage of MOFs. The confinement effects in the nanocage of MOFs will shorten the distance between the molecules, and the catalytic pathway of water oxidation may be changed. However, the match in the positions and directions of the two Ru active sites anchored on the cage is difficult. Compared with dinuclear Ru complex D-Ru, the EXAFS results showed that no analogue of dinuclear Ru complex was formed in the cage of catalyst **3** (Fig. S32). Therefore, the water nucleophilic attack pathway claimed previously is more consistent for these molecular Ru analogues in MOFs [73].

Although MIL-101(Cr) does not show catalytic activity at all, the Cr cations in MIL-101(Cr) could act as electron relays between the catalytic center of Ru and the oxidant of Ce^{IV} (Fig. S33). When the Ce^{IV} solution was added into the suspension of catalyst **3** or pure MIL-101(Cr) (Fig. S34), a set of narrow EPR bands assigned for Cr^{V} was observed at g = 1.97 for catalyst **3** while no EPR signal of Cr^{V} was detected for pure MIL-101(Cr) [74]. Therefore, Cr^{III} in pure MOFs cannot be directly oxidized to Cr^{V} by Ce^{IV}, and the electron transfer between Ru complex and the framework of MOFs could be the real reason for the formation of Cr^{V} in the framework of catalyst **3**. The valences of Cr in MOFs are kept as +3 valence state before and after reaction (Fig. S35), revealing the valences of Cr recovered from higher valence to +3 when the reaction was finished. Therefore, the framework of MOFs acts as the stabilizing support with the function of storing and donating electrons for Ru complex segments in catalyst **3**-**5**. The electronic effect of framework in MOFs plays an important role in the enhancement of catalytic water oxidation.

The change of coordination environment for hybrid catalysts could further improve the catalytic activity. To clarify the structural change of **3** during water oxidation reaction, the recovered catalyst **3** after the first run was measured by XAS spectra. From the wavelet transform of χ(k) spectrum of recovered **3** (Fig. S36), the scattering path signal located at [χ(k), χ(R)] of [5, 1.86] is assigned to Ru—N, and the weak signal located at [χ(k), χ(R)] of [8.6, 2.42] is Ru—O, revealing that the coordination environment of Ru atoms in recovered **3** contain Ru—N and Ru—O, which is further supported by the EXAFS results. As shown in Fig. 9, the EXAFS spectrum of recovered **3** can be adequately fitted by the DFT-optimized structure model of $[Ru(terpy\text{-}Ac\text{-}NH_2)(pic)_2(H_2O)]^{2+}$(Fig. 9c) while significant deviation was observed based on the structure model of $[Ru(terpy\text{-}Ac\text{-}NH_2)(pic)_2Cl]^{+}$. Thereby, the equatorial chloro ligand of Ru unit in catalyst **3** was replaced by the H_2O, which is consistent with the shift of Ru $3d_{5/2}$ peak in XPS (Fig. 7b). The replacement of Cl^- as H_2O improves the water oxidation activity of catalyst **3** during the reaction (Fig. 10a). In all, a new species with $[Ru{-}OH_2]$ structure are responsible for the high oxygen evolution activity according to the analysis of the above EXAFS spectra and XPS analysis. As a matter of fact, the coordinated H_2O in molecular Ru complex was proved to greatly influence the oxygen evolution ability [75,76]. In addition, $[Ru(terpy)(bpy)(OH_2)]^{2+}$ has been verified to be a highly active and fairly stable water oxidation catalyst while $[Ru(terpy)(bpy)Cl]^{+}$ exhibited no activity at all [77]. In conclusion, the Ru complex with the structural unit $[Ru{-}OH_2]$ for recovered **3** is the real water oxidation catalyst.

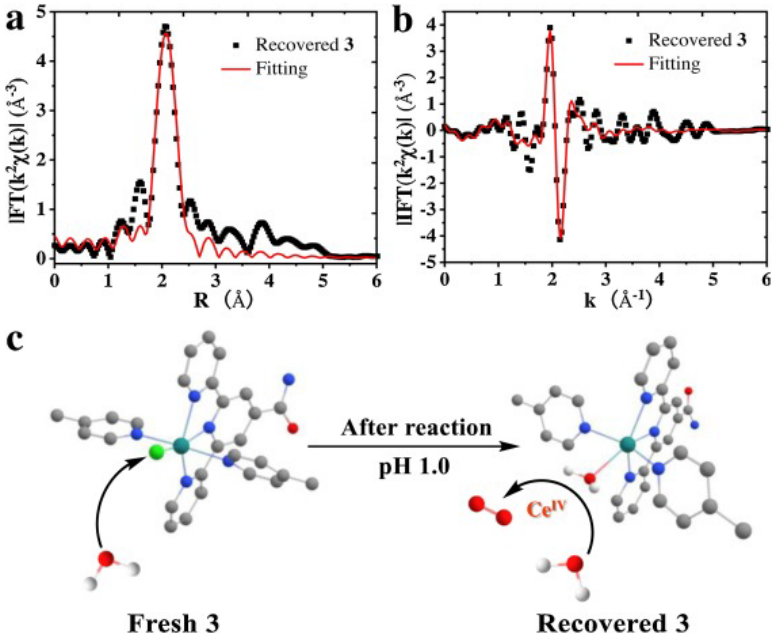

Fig. 9. (a) χ(R) space spectra fitting curve of recovered 3. (b) Inverse FT χ(R) space spectra into χ(q) space spectra (χ(k) space) fitting curve of recovered 3. (c) DFT-optimized molecular model $[Ru(terpy\text{-}Ac\text{-}NH_2)(pic)_2(H_2O)]^{2+}$ (right), Cl is substituted by H_2O in Ru complex of catalyst 3, C (gray), H (light gray), O (red), N (blue), Ru (dark cyan), Cl (green) (For interpretation of the references to colour in this figure legend, the reader is referred to the web version of this article.).

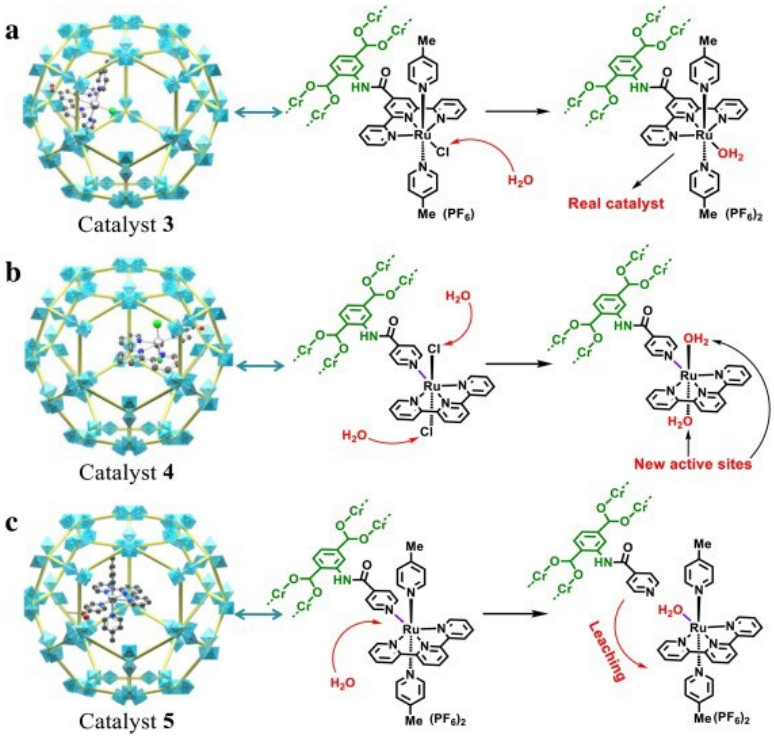

Fig. 10. The speculations for the huge differences in water oxidation activity and recycle stability among these hybrid catalysts.

The covalent immobilization of hybrid catalysts provides a promising way to investigate the relationship among the activity, stability and the structure of molecular catalysts. Some homogeneous water oxidation catalysts have short longevity due to the serious intermolecular oxidative decomposition. When the homogeneous catalysts were anchored in the cages of MOFs, the molecular catalysts were separated from each other, which could effectively avoid such intermolecular decomposition. Hence, with the anchoring of molecular complexes, the obtained hybrid catalysts generally show improvement in catalytic stability and activity. However, only catalyst **3** of three hybrid heterogeneous catalysts showed significant enhancement in water oxidation activity. In addition to the ability to avoid intermolecular oxidative decomposition, catalyst **3** has the following unique advantages: (1) a highly efficient water oxidation pre-catalyst $[Ru(terpy\text{-}Ac)(pic)_2Cl]^+$ is in situ formed in cages of MIL-101(Cr) (labeled as **3**) instead of $[Ru(terpy\text{-}Ac)(pic)_3]^{2+}$ (homogeneous catalyst **2**) when the geometric confinement effect of MOFs is utilized; (2) a higher active species $[Ru(terpy\text{-}Ac)(pic)_2(H_2O)]^{2+}$ is generated during water oxidation for catalyst **3** due to the exchange in equatorial ligands; (3) the activity of the Ru complex is greatly enhanced due to the electron donor effect of the frameworks in MOFs; (4) the stable anchoring ensures the high catalytic activity of the catalyst in the system.

A significant difference in recycle stability of water oxidation was observed between catalysts **4** and **5**. For catalyst **4**, the Ru moieties are well maintained as evidenced by its robust catalytic activity in recycle tests (Fig. 8b). The continuous loss of activity of recycle tests for catalyst **5** (Fig. 8c) revealed the leaching of Ru molecular complexes. In addition, 10.2 μM Ru was detected in the supernatant of **5** after the first run, which further confirmed the leaching of the Ru complexes from the frameworks of MIL-101(Cr). The only difference of Ru complexes between **4** and **5** is that Cl is the axial ligand for **4** while pic is the axial ligand for **5**. The significant difference in recycle stability between catalysts **4** and **5** indicates that two axial ligands play an important role for the stability of hybrid catalysts. The negative shift of Ru $3d_{5/2}$ peak in **4** after reaction could be caused by the change of coordination environments (Fig. S30b). As we mentioned above, the negative shift of Ru $3d_{5/2}$ peak in the recovered catalyst **3** was due to the substitution of Cl^- by H_2O. The axial chloro ligand in catalyst **4** is more

easily replaced than the equatorial ligand pyridine. Hence, the structure unit of [Ru−OH_2] could be formed in recovered catalyst **4**. The ligands of isc in both catalysts **4** and **5** are one of the important bridges connecting molecular Ru catalyst fragment to the framework of MOFs. Two Cl ligands in **4** could be replaced by two H_2O molecules to afford two active sites in the axial positions, thus protecting the Ru─N coordination bond between bridging ligand isc and Ru from being attacked by H_2O (Fig. 10b). Therefore, the Ru complexes are stably anchored to the frameworks of catalyst **4**. As the axial pic ligand of catalyst **5** is difficult to be replaced by H_2O, the bridging isc ligand in equatorial plane will be substituted by H_2O. The Ru complex segments in hybrid catalyst **5** easily fall off the frameworks of MOFs (Fig. 10c), resulting in the poor recycle stability for catalyst **5**.

It is difficult for the catalytic species of homogeneous catalysts to be clearly and directly clarified due to the reason that molecular catalyst dissolved in solution is hard to be recycled and studied in detail. The covalent immobilization of homogeneous catalysts is a good way to resolve this problem. We found that $[Ru(terpy\text{-}Ac)(pic)_2(H_2O)]^{2+}$ is the real catalyst in catalyst **3** through the characterization of XAS and XPS analysis. In addition, the covalent immobilization of homogeneous catalysts is an excellent strategy to achieve difficult directional synthesis. For homogeneous catalysts $[Ru(terpy)(pic)_3]^{2+}$ and its analogues, it is difficult to only change the axial ligand pic without altering the equatorial ligand pic. By taking the substitutable ligand in equatorial plane as the bridge, we realized the directional modulation of the axial ligands and obtained the $[Ru(terpy)(sic)Cl_2]^{2+}$ and $[Ru(terpy)(sic)(pic)_2]^{2+}$ in the frameworks of MIL-101(Cr) for catalysts **4** and **5.** The key rule of the axial ligands in the recycle stability for hybrid catalysts was obtained by comparing the stability in recycle tests between catalysts **4** and **5**.

4. Conclusion

Three novel hybrid catalysts were successfully synthesized through the covalent immobilization of noble metal complexes on the frameworks of MIL-101(Cr). The structural information of these catalysts was fully investigated by XAS and XPS analysis. Robust catalyst **3** exhibited high water oxidation activity in the Ce^{IV}-driven system, which was 120 times higher than that of homogeneous Ru complex. Geometric confinement and electronic effect of MOFs results in extraordinarily high catalytic activity of catalyst **3**. Our experimental results provide the solid evidence that the Ru-aqua species, $[Ru(terpy)(pic)_2(OH_2)]^{2+}$, is the real water oxidation catalyst. The recycle of noble metal-based molecular catalysts was well realized by catalysts **3** and **4**. The vital function of the axial ligands in the recycle stability for hybrid catalysts was obtained by comparing the structure and recycle stability between catalysts **4** and **5**. The poor recycle stability of catalyst **5** is due to the fact that Ru complex segments fall off the frameworks of MOFs. The axial ligands Cl^- of Ru complexes in catalyst **4** are more easily replaced than the axial ligands pic of Ru complexes in catalyst **5**, which could provide new active sites for water oxidation and protect the Ru─N coordination bond between bridging ligand isc and Ru from being attacked by H_2O. For this reason, the Ru complexes in catalyst **4** are well retained in recycle tests. The catalytic species of homogeneous catalysts are difficult to be clearly and directly clarified due to the challenge of recycling catalysts. This work not only realizes the heterogeneous transformation of homogeneous Ru complexes to be easily recycled and identified, but also provides a new synthetic strategy to improve the stability and activity of the hybrid catalysts.

CRediT authorship contribution statement

Xiangming Liang: Data curation, Investigation, Writing - original draft. **Sizhuo Yang:** Investigation. **Junyi Yang:** Data curation, Validation. **Wanjun Sun:** Formal analysis. **Xiangyang Li:** Visualization. **Baochun Ma:** Methodology. **Jier Huang:** Formal analysis, Resources. **Jiangwei Zhang:** Data curation, Writing - review & editing. **Lele Duan:** Formal analysis, Writing - review & editing. **Yong Ding:** Project administration, Supervision, Writing - review & editing.

Declaration of Competing Interest

The authors report no declarations of interest.

Acknowledgements

This work was financially supported by the National Natural Science Foundation of China (Grants No. 21773096, 22075119, 21701168). We gratefully acknowledge BL14W1 beamline of Shanghai Synchrotron Radiation Facility (SSRF) Shanghai, China and 1W1B, 1W2B beamline of Beijing Synchrotron Radiation Facility (BSRF) Beijing, China for providing the beam time. The financial support from the National Key Basic Research Program of China (2020YFA0406101), Liaoning Natural Science Foundation (20180510050), Dalian high level talent innovation project(2019RQ063). Use of the Advanced Photon Source in Argonne National Laboratory was supported by the U. S. Department of Energy, Office of Science, Office of Basic Energy Sciences, under Award No. DE-AC02-06CH11357.

References

1. N.S. Lewis, D.G. Nocera, **Powering the planet: chemical challenges in solar energy utilization,** Proc. Natl. Acad. Sci. U. S. A., 103 (2006), pp. 15729-15735
2. M. Yagi, M. Kaneko, **Molecular catalysts for water oxidation,** Chem. Rev., 101 (2001), pp. 21-35
3. N. Armaroli, V. Balzani, **The future of energy supply: challenges and opportunities,** Angew. Chem. Int. Ed., 46 (2007), pp. 52-66
4. A.J. Bard, M.A. Fox, **Artificial photosynthesis solar splitting of water to hydrogen and oxygen,** Acc. Chem. Res., 28 (1995), pp. 141-145
5. S. Chu, A. Majumdar, **Opportunities and challenges for a sustainable energy future,** Nature, 488 (2012), pp. 294-303
6. X. Du, J. Zhao, J. Mi, Y. Ding, P. Zhou, B. Ma, J. Zhao, J. Song, **Efficient photocatalytic H_2 evolution catalyzed by an unprecedented robust molecular semiconductor {Fe11} nanocluster without cocatalysts at neutral conditions,** Nano Energy, 16 (2015), pp. 247-255
7. X. Liang, J. Lin, X. Cao, W. Sun, J. Yang, B. Ma, Y. Ding, **Enhanced photocatalytic activity of $BiVO_4$ coupled with iron-based complexes for water oxidation under visible light irradiation,** Chem. Commun., 55 (2019), pp. 2529-2532
8. M.W. Kanan, D.G. Nocera, **In situ formation of an oxygen-evolving catalyst in neutral water containing phosphate and Co^{2+},** Science, 321 (2008), pp. 1072-1075
9. F. Song, Y. Ding, B. Ma, C. Wang, Q. Wang, X. Du, S. Fu, J. Song, **$K_7[Co^{III}Co^{II}(H_2O)W_{11}O_{39}]$: A molecular mixed-valence keggin polyoxometalate catalyst of high stability and efficiency for visible light-driven water oxidation,** Energy Environ. Sci., 6 (2013), pp. 1170-1184
10. M. Zheng, Y. Ding, X. Cao, T. Tian, J. Lin, **Homogeneous and heterogeneous photocatalytic water oxidation by polyoxometalates containing the most earth-abundant transition metal, iron,** Appl. Catal. B: Environ., 237 (2018), pp. 1091-1100
11. J. Lin, X. Meng, M. Zheng, B. Ma, Y. Ding, **Insight into a hexanuclear cobalt complex: strategy to construct efficient catalysts for visible light-driven water oxidation,** Appl. Catal. B: Environ., 241 (2019), pp. 351-358
12. X. Wu, F. Li, B. Zhang, L. Sun, **Molecular complexes in water oxidation: pre-catalysts or real catalysts,** J. Photoch. Photobio. C: Photoch. Rev., 25 (2015), pp. 71-89
13. X. Liang, X. Cao, W. Sun, Y. Ding, **Recent progress in visible light driven water oxidation using semiconductors coupled with molecular catalysts,** ChemCatChem, 11 (2019), pp. 6190-6202

14. J. Chen, X. Tao, C. Li, Y. Ma, L. Tao, D. Zheng, J. Zhu, H. Li, R. Li, Q. Yang, **Synthesis of bipyridine-based covalent organic frameworks for visible-light-driven photocatalytic water oxidation,** Appl. Catal. B: Environ., 262 (2020), Article 118271
15. W. Sun, X. Meng, C. Xu, J. Yang, X. Liang, Y. Dong, C. Dong, Y. Ding, **Amorphous CoO_x coupled carbon dots as a spongy porous bifunctional catalyst for efficient photocatalytic water oxidation and CO_2 reduction,** Chin. J. Catal., 41 (2020), pp. 1826-1836
16. Y.-J. Yuan, Z.-K. Shen, P. Wang, Z. Li, L. Pei, J. Zhong, Z. Ji, Z.-T. Yu, Z. Zou, **Metal-free broad-spectrum PTCDA/g-C_3N_4 Z-scheme photocatalysts for enhanced photocatalytic water oxidation,** Appl. Catal. B: Environ., 260 (2020), Article 118179
17. M. Hara, C.C. Waraksa, J.T. Lean, B.A. Lewis, T.E. Mallouk, **Photocatalytic water oxidation in a buffered tris(2,2'-bipyridyl)ruthenium complex-colloidal IrO_2 system,** J. Phys. Chem. A, 104 (2000), pp. 5275-5280
18. F.A. Frame, T.K. Townsend, R.L. Chamousis, E.M. Sabio, T. Dittrich, N.D. Browning, F.E. Osterloh, **Photocatalytic water oxidation with nonsensitized IrO_2nanocrystals under visible and UV light,** J. Am. Chem. Soc., 133 (2011), pp. 7264-7267
19. R.D.L. Smith, M.S. Prévot, R.D. Fagan, Z. Zhang, P.A. Sedach, M.K.J. Siu, S. Trudel, C.P. Berlinguette, **Photochemical route for accessing amorphous metal oxide materials for water oxidation catalysis,** Science, 340 (2013), pp. 60-63
20. H. Zhang, W. Tian, L. Zhou, H. Sun, M. Tade, S. Wang, **Monodisperse Co_3O_4 quantum dots on porous carbon nitride nanosheets for enhanced visible-light-driven water oxidation,** Appl. Catal. B: Environ., 223 (2018), pp. 2-9
21. J. Hao, W. Yang, Z. Peng, C. Zhang, Z. Huang, W. Shi, **A nitrogen doping method for CoS_2 electrocatalysts with enhanced water oxidation performance,** ACS Catal., 7 (2017), pp. 4214-4220
22. J. Hao, W. Yang, J. Hou, B. Mao, Z. Huang, W. Shi, **Nitrogen doped NiS_2nanoarrays with enhanced electrocatalytic activity for water oxidation,** J. Mater. Chem. A, 5 (2017), pp. 17811-17816
23. W. Kong, X. Luan, H.Y. Du, L. Xia, F. Qu, **Enhanced electrocatalytic activity of water oxidation in an alkaline medium via Fe doping in CoS_2 nanosheets,** Chem. Commun., 55 (2019), pp. 2469-2472
24. X. Luan, H.Y. Du, Y. Kong, F. Qu, L. Lu, **A novel FeS-NiS hybrid nanoarray: an efficient and durable electrocatalyst for alkaline water oxidation,** Chem. Commun., 55 (2019), pp. 7335-7338
25. Y. Naruta, M. Sasayama, T. Sasaki, **Oxygen evolution by oxidation of water with manganese porphyrin dimers,** Angew. Chem. Int. Ed., 33 (1994), pp. 1839-1841
26. N.D. McDaniel, F.J. Coughlin, L.L. Tinker, S. Bernhard, **Cyclometalated iridium(III) aquo complexes: efficient and tunable catalysts for the homogeneous oxidation of water,** J. Am. Chem. Soc., 130 (2008), pp. 210-217
27. W.C. Ellis, N.D. McDaniel, S. Bernhard, T.J. Collins, **Fast water oxidation using iron,** J. Am. Chem. Soc., 132 (2010), pp. 10990-10991
28. D.J. Wasylenko, C. Ganesamoorthy, J. Borau-Garcia, C.P. Berlinguette, **Electrochemical evidence for catalytic water oxidation mediated by a high-valent cobalt complex,** Chem. Commun., 47 (2011), pp. 4249-4251
29. S.M. Barnett, K.I. Goldberg, J.M. Mayer, **A soluble copper-bipyridine water-oxidation electrocatalyst,** Nature Chem., 4 (2012), pp. 498-502
30. M. Zhang, M.T. Zhang, C. Hou, Z.F. Ke, T.B. Lu, **Homogeneous electrocatalytic water oxidation at neutral pH by a robust macrocyclic nickel(II) complex,** Angew. Chem. Int. Ed., 53 (2014), pp. 13042-13048
31. Y.V. Geletii, Z. Huang, Y. Hou, D.G. Musaev, T. Lian, C.L. Hill, **Homogeneous light-driven water oxidation catalyzed by a tetraruthenium complex with all inorganic ligands,** J. Am. Chem. Soc., 131 (2009), pp. 7522-7523

32. Q. Yin, J.M. Tan, C. Besson, Y.V. Geletii, D.G. Musaev, A.E. Kuznetsov, Z. Luo, K.I. Hardcastle, C.L. Hill, **A fast soluble carbon-free molecular water oxidation catalyst based on abundant metals,** Science, 328 (2010), pp. 342-345
33. Z. Huang, Z. Luo, Y.V. Geletii, J.W. Vickers, Q. Yin, D. Wu, Y. Hou, Y. Ding, J. Song, D.G. Musaev, C.L. Hill, T . Lian, **Efficient light-driven carbon-free cobalt-based molecular catalyst for water oxidation,** J. Am. Chem. Soc., 133 (2011), pp. 2068-2071
34. H. Lv, J. Song, Y.V. Geletii, J.W. Vickers, J.M. Sumliner, D.G. Musaev, P. Kogerler, P.F. Zhuk, J. Bacsa, G. Zh u, C.L. Hill, **An exceptionally fast homogeneous carbon-free cobalt-based water oxidation catalyst,** J. Am. Chem. Soc., 136 (2014), pp. 9268-9271
35. J. Soriano-López, D.G. Musaev, C.L. Hill, J.R. Galán-Mascarós, J.J. Carbó, J.M. Poblet, **Tetracobalt-polyoxometalate catalysts for water oxidation: key mechanistic details,** J. Catal., 350 (2017), pp. 56-63
36. Y. Cong, H.S. Park, H.X. Dang, F.F. Fan, A.J. Bard, C.B. Mullins, **Tantalum cobalt nitride photocatalysts for water oxidation under visible light,** Chem. Mater., 24 (2012), pp. 579-586
37. D. Hong, Y. Yamada, T. Nagatomi, Y. Takai, S. Fukuzumi, **Catalysis of nickel ferrite for photocatalytic water oxidation using $[Ru(bpy)_3]^{2+}$ and $S_2O_8^{2-}$,** J. Am. Chem. Soc., 134 (2012), pp. 19572-19575
38. F. Jiao, H. Frei, **Nanostructured cobalt oxide clusters in mesoporous silica as efficient oxygen-evolving catalysts,** Angew. Chem. Int. Ed., 48 (2009), pp. 1841-1844
39. B.M. Hunter, H.B. Gray, A.M. Muller, **Earth-abundant heterogeneous water oxidation catalysts,** Chem. Rev., 116 (2016), pp. 14120-14136
40. H.-W. Tseng, R. Zong, J.T. Muckerman, R. Thummel, **Mononuclear ruthenium(II) complexes that catalyze water oxidation,** Inorg. Chem., 47 (2008), pp. 11763-11773
41. M.T. Zhang, Z. Chen, P. Kang, T.J. Meyer, **Electrocatalytic water oxidation with a copper(II) polypeptide complex,** J. Am. Chem. Soc., 135 (2013), pp. 2048-2051
42. L. Wang, L. Duan, R.B. Ambre, Q. Daniel, H. Chen, J. Sun, B. Das, A. Thapper, J. Uhlig, P. Dinér, L. Sun, **A nickel (II) PY5 complex as an electrocatalyst for water oxidation,** J. Catal., 335 (2016), pp. 72-78
43. Q. Han, D. Sun, J. Zhao, X. Liang, Y. Ding, **A novel di-cobalt-substituted tungstoantimonate polyoxometalate: synthesis, characterization and photocatalytic water oxidation properties,** Chin. J. Catal., 40 (2019), pp. 953-958
44. R. Matheu, M.Z. Ertem, C. Gimbert-Surinach, X. Sala, A. Llobet, **Seven coordinated molecular ruthenium-water oxidation catalysts: a coordination chemistry journey,** Chem. Rev., 119 (2019), pp. 3453-3471
45. S.W. Gersten, G.J. Samuels, T.J. Meyer, **Catalytic oxidation of water by an oxo-bridged ruthenium dimer,** J. Am. Chem. Soc., 104 (1982), pp. 4029-4030
46. L. Duan, A. Fischer, Y. Xu, L. Sun, **Isolated seven-coordinate Ru(IV) dimer complex with [HOHOH]- bridging ligand as an intermediate for catalytic water oxidation,** J. Am. Chem. Soc., 131 (2009), pp. 10397-10399
47. R. Zong, R.P. Thummel, **A new family of Ru complexes for water oxidation,** J. Am. Chem. Soc., 127 (2005), pp. 12802-12803
48. J.J. Concepcion, J.W. Jurss, J.L. Templeton, T.J. Meyer, **One site is enough. Catalytic water oxidation by $[Ru(tpy)(bpm)(OH_2)]^{2+}$ and $[Ru(tpy)(bpz)(OH_2)]^{2+}$,** J. Am. Chem. Soc., 130 (2008), pp. 16462-16463
49. L. Duan, F. Bozoglian, S. Mandal, B. Stewart, T. Privalov, A. Llobet, L. Sun, **A molecular ruthenium catalyst with water-oxidation activity comparable to that of photosystem II,** Nature Chem., 4 (2012), pp. 418-423
50. Y. Jiang, F. Li, B. Zhang, X. Li, X. Wang, F. Huang, L. Sun, **Promoting the activity of catalysts for the oxidation of water with bridged dinuclear ruthenium complexes,** Angew. Chem. Int. Ed., 52 (2013), pp. 3398-3401

51. G. Chen, L. Chen, S.-M. Ng, W.-L. Man, T.-C. Lau, **Chemical and visible-light-driven water oxidation by iron complexes at pH 7-9: evidence for dual-active intermediates in iron catalyzed water oxidation,** Angew. Chem. Int. Ed., 52 (2013), pp. 1789-1791
52. A.I. Nguyen, K.M.V. Allsburg, M.W. Terband, M. Bajdich, J. Oktawiec, J. Amtawong, M.S. Ziegler, J.P. Dom browski, K.V. Lakshmif, W.S. Drisdell, J. Yano, S.J.L. Billing, T.D. Tilley, **Stabilization of reactive Co_4O_4cubane oxygen catalysts within porous frameworks,** Proc. Natl. Acad. Sci. U. S. A., 116 (2019), pp. 11630-11639
53. C. Wang, J.L. Wang, W. Lin, **Elucidating molecular iridium water oxidation catalysts using metal-organic frameworks: a comprehensive structural, catalytic, spectroscopic, and kinetic study,** J. Am. Chem. Soc., 134 (2012), pp. 19895-19908
54. S. Lin, A.K. Ravari, J. Zhu, P.M. Usov, M. Cai, S.R. Ahrenholtz, Y. Pushkar, A.J. Morris, **Insight into metal-organic framework reactivity: chemical water oxidation catalyzed by a $[Ru(tpy)(dcbpy)(OH_2)]^{2+}$ modified UiO-67,** ChemSusChem, 11 (2018), pp. 464-471
55. R. Ezhov, A. Karbakhsh Ravari, A. Page, Y. Pushkar, **Water oxidation catalyst cis-$[Ru(bpy)(5,5'-dcbpy)(H_2O)_2]^{2+}$ and its stabilization in metal-organic framework,** ACS Catal., 10 (2020), pp. 5299-5308
56. G. Férey, C. Mellot-Draznieks, C. Serre, F. Millange, J. Dutour, S. Surblé, I. Margiolaki, **A chromium terephthalate-based solid with unusually large pore volumes and surface area,** Science, 309 (2005), pp. 2040-2042
57. H.-W. Tseng, R. Zong, J.T. Muckerman, R. Thummel, **Mononuclear ruthenium(II) complexes that catalyze water oxidation,** Inorg. Chem., 47 (2008), pp. 11763-11773
58. S. Rostamnia, H. Alamgholiloo, M. Jafari, **Ethylene diamine post-synthesis modification on open metal site Cr-MOF to access efficient bifunctional catalyst for the hantzsch condensation reaction,** Appl. Organometal. Chem., 32 (2018), p. e4370
59. K. Getty, M.U. Delgado-Jaime, P. Kennepohl, **Assignment of pre-edge features in the Ru K-edge X-ray absorption spectra of organometallic ruthenium complexes,** Inorg. Chim. Acta, 361 (2008), pp. 1059-1065
60. H. Hashizume, K. Ishiji, J.C. Lang, D. Haskel, G. Srajer, J. Minár, H. Ebert, **Observation of X-ray magnetic circular dichroism at the Ru K edge in Co-Ru alloys,** Phys. Rev. B, 73 (2006), Article 224416
61. Y. Han, Y. Wang, R. Xu, W.L. Chen, L. Zheng, A. Han, Y. Zhu, J. Zhang, H. Zhang, J. Luo, C. Chen, Q. Peng, D . Wang, Y. Li, **Electronic structure engineering to boost oxygen reduction activity by controlling the coordination of the central metal,** Energy Environ. Sci., 11 (2018), pp. 2348-2352
62. L. Zhang, J. Chen, T. Fan, K. Shen, M. Jiang, Y. Li, **A high-valent di-μ-oxo dimanganese complex covalently anchored in a metal-organic framework as a highly efficient and recoverable water oxidation catalyst,** Chem. Commun., 54 (2018), pp. 4188-4191
63. V. Mazzieri, F. Coloma-Pascualb, A. Arcoyac, P.C.L.' Argentièrea, N.S. FÍgolia, **XPS, FTIR and TPR characterization of Ru/Al_2O_3 catalysts,** Appl. Surf. Sci., 210 (2003), pp. 222-230
64. M. Tada, R. Coquet, J. Yoshida, M. Kinoshita, Y. Iwasawa, **Selective formation of a coordinatively unsaturated metal complex at a surface: a SiO_2-immobilized, three-coordinate ruthenium catalyst for alkene epoxidation,** Angew. Chem. Int. Ed., 46 (2007), pp. 7220-7223
65. D. Frath, V.Q. Nguyen, F. Lafolet, P. Martin, J.-C. Lacroix, **Electrografted monolayer based on a naphthalene diimide-ruthenium terpyridine complex dyad: efficient creation of large-area molecular junctions with high current densities,** Chem. Commun., 53 (2017), pp. 10997-11000
66. X. You, G. Zou, Q. Ye, Q. Zhang, P. He, **Ruthenium(II) complex-sensitized solid-state polymerization of diacetylene in the visible light region,** J. Mater. Chem., 18 (2008), pp. 4704-4711
67. N. Zhang, M. Qi, L. Yuan, X. Fu, Z. Tang, J. Gong, Y. Xu, **Broadband light harvesting and unidirectional electron flow for efficient electron accumulation for hydrogen generation,** Angew. Chem. Int. Ed., 58 (2019), pp. 10003-10007

68. M. Saikia, L. Saikia, **Palladium nanoparticles immobilized on an amine-functionalized MIL-101(Cr) as a highly active catalyst for oxidative amination of aldehydes,** RSC Adv., 6 (2016), pp. 14937-14947
69. M. Trzebiatowska-Gusowska, A. Gągor, E. Coetsee, E. Erasmus, H.C. Swart, J.C. Swarts, **Nano islet formation of formyl- and carboxyferrocene, -ruthenocene, -osmocene and cobaltocenium on amine-functionalized silicon wafers highlighted by crystallographic, AFM and XPS studies,** J. Organomet. Chem., 745 (2013), pp. 393-403
70. Y. Li, S. Li, J. Zhu, A. Volodine, B.V. Bruggen, **Controllable synthesis of a chemically stable molecular sieving nanofilm for highly efficient organic solvent nanofiltration,** Chem. Sci., 11 (2020), pp. 4263-4271
71. X. Wang, Y. Wu, X. Zhou, J. Xiao, Q. Xia, H. Wang, Z. Li, **Novel C-PDA adsorbents with high uptake and preferential adsorption of ethane over ethylene,** Chem. Eng. Sci., 155 (2016), pp. 338-347
72. R.E. Hansen, S. Das, **Biomimetic di-manganese catalyst cage-isolated in a MOF: robust catalyst for water oxidation with Ce(IV), a non-O-donating oxidant,** Energy Environ. Sci., 7 (2014), pp. 317-322
73. L. Duan, Y. Xu, L. Tong, L. Sun, **Ce^{IV}- and light-driven water oxidation by $[Ru(terpy)(pic)_3]^{2+}$ analogues: catalytic and mechanistic studies,** ChemSusChem, 4 (2011), pp. 238-244
74. S. Khaddar-Zine, A. Ghorbel, C. Naccache, **EPR and UV-visible spectroscopic studies of alumina-supported chromium oxide catalysts,** J. Mol. Catal. A Chem., 150 (1999), pp. 223-231
75. Y. Pushkar, D. Moonshiram, V. Purohit, L. Yan, I. Alperovich, **Spectroscopic analysis of catalytic water oxidation by $[Ru(II)(bpy)(tpy)H_2O]^{2+}$ suggests that Ru^{V}=O is not a rate-limiting intermediate,** J. Am. Chem. Soc., 136 (2014), pp. 11938-11945
76. L. Yan, R. Zong, Y. Pushkar, **Unexpected ligand lability in condition of water oxidation catalysis,** J. Catal., 330 (2015), pp. 255-260
77. S. Masaoka, K. Sakai, **Clear evidence showing the robustness of a highly active oxygen-evolving mononuclear ruthenium complex with an aqua ligand,** Chem. Lett., 38 (2009), pp. 182-183